



**NAVAL
POSTGRADUATE
SCHOOL**

MONTEREY, CALIFORNIA

THESIS

**FEASIBILITY OF HIGH ENERGY LASERS FOR
INTERDICTION ACTIVITIES**

by

Carlos Abel Javier Romero Chero

December 2017

Thesis Advisor:

Keith Cohn

Co-Advisor:

Joseph Blau

Approved for public release. Distribution is unlimited.

THIS PAGE INTENTIONALLY LEFT BLANK

REPORT DOCUMENTATION PAGE			<i>Form Approved OMB No. 0704-0188</i>	
Public reporting burden for this collection of information is estimated to average 1 hour per response, including the time for reviewing instruction, searching existing data sources, gathering and maintaining the data needed, and completing and reviewing the collection of information. Send comments regarding this burden estimate or any other aspect of this collection of information, including suggestions for reducing this burden to Washington headquarters Services, Directorate for Information Operations and Reports, 1215 Jefferson Davis Highway, Suite 1204, Arlington, VA 22202-4302, and to the Office of Management and Budget, Paperwork Reduction Project (0704-0188) Washington DC 20503.				
1. AGENCY USE ONLY (Leave Blank)		2. REPORT DATE December 2017	3. REPORT TYPE AND DATES COVERED Master's Thesis	
4. TITLE AND SUBTITLE FEASIBILITY OF HIGH ENERGY LASERS FOR INTERDICTION ACTIVITIES			5. FUNDING NUMBERS	
6. AUTHOR(S) Carlos Abel Javier Romero Chero				
7. PERFORMING ORGANIZATION NAME(S) AND ADDRESS(ES) Naval Postgraduate School Monterey, CA 93943			8. PERFORMING ORGANIZATION REPORT NUMBER	
9. SPONSORING / MONITORING AGENCY NAME(S) AND ADDRESS(ES) N/A			10. SPONSORING / MONITORING AGENCY REPORT NUMBER	
11. SUPPLEMENTARY NOTES The views expressed in this document are those of the author and do not reflect the official policy or position of the Department of Defense or the U.S. Government. IRB Protocol Number: NA.				
12a. DISTRIBUTION / AVAILABILITY STATEMENT Approved for public release. Distribution is unlimited.			12b. DISTRIBUTION CODE	
13. ABSTRACT (maximum 200 words) One of the greatest threats to Peru as a nation is the increasing amount of illicit activities in recent years. Among them all, drug trafficking causes the most damage within and outside of Peru's borders. Therefore, interdiction of these activities is paramount for the Peruvian Navy, since this institution is responsible for all the bodies of water where Peru has jurisdiction. There are multiple ways to perform interdiction, but few of them can be done without damaging the people or cargo. High Energy Laser (HEL) weapons are an effective way to deliver energy precisely from a relative long range. This thesis studies the feasibility of the usage of this kind of weapon, fired from a surface or an unmanned aerial vehicle platform, against the water crafts that are used to deliver the illicit material from the Peruvian coast to a ship waiting offshore. Specifically, dwell times will be estimated to melt through vulnerable spots in the target for different HEL configurations.				
14. SUBJECT TERMS directed energy, lasers, atmospheric propagation, interdiction, Peruvian Navy			15. NUMBER OF PAGES 69	
			16. PRICE CODE	
17. SECURITY CLASSIFICATION OF REPORT Unclassified	18. SECURITY CLASSIFICATION OF THIS PAGE Unclassified	19. SECURITY CLASSIFICATION OF ABSTRACT Unclassified	20. LIMITATION OF ABSTRACT UU	

THIS PAGE INTENTIONALLY LEFT BLANK

Approved for public release. Distribution is unlimited.

FEASIBILITY OF HIGH ENERGY LASERS FOR INTERDICTION ACTIVITIES

Carlos Abel Javier Romero Chero
Lieutenant Junior Grade, Peruvian Navy
B.S., Peruvian Naval Academy, 2012
B.S., University of Piura, 2012

Submitted in partial fulfillment of the
requirements for the degree of

MASTER OF SCIENCE IN APPLIED PHYSICS

from the

**NAVAL POSTGRADUATE SCHOOL
December 2017**

Approved by: Keith Cohn
Thesis Advisor

Joseph Blau
Thesis Co-Advisor

Kevin Smith
Chair, Department of Physics

THIS PAGE INTENTIONALLY LEFT BLANK

Abstract

One of the greatest threats to Peru as a nation is the increasing amount of illicit activities in recent years. Among them all, drug trafficking causes the most damage within and outside of Peru's borders. Therefore, interdiction of these activities is paramount for the Peruvian Navy, since this institution is responsible for all the bodies of water where Peru has jurisdiction. There are multiple ways to perform interdiction, but few of them can be done without damaging the people or cargo. High Energy Laser (HEL) weapons are an effective way to deliver energy precisely from a relative long range. This thesis studies the feasibility of the usage of this kind of weapon, fired from a surface or an unmanned aerial vehicle platform, against the water crafts that are used to deliver the illicit material from the Peruvian coast to a ship waiting offshore. Specifically, dwell times will be estimated to melt through vulnerable spots in the target for different HEL configurations.

THIS PAGE INTENTIONALLY LEFT BLANK

Table of Contents

1	Introduction to Peruvian Navy Operations	1
1.1	Peruvian Navy History	1
1.2	Peruvian Navy Today	2
1.3	Peruvian Navy Responsibilities	2
1.4	Motivation for Directed Energy Employment for Interdiction	4
2	Directed Energy Overview	7
2.1	Introduction to Directed Energy	7
2.2	High Energy Lasers Classification	8
2.3	Laser Weapon Performance Metrics	10
2.3.1	Irradiance	11
2.3.2	Power in the Bucket	11
2.3.3	Dwell Time	11
3	Target Damage Physics	13
3.1	Laser Heating of Materials and Conductive Losses	13
3.2	Laser Induced Melting	15
3.2.1	Assumptions.	16
3.2.2	Real Life Effects	16
3.2.3	Boundary Conditions.	17
3.2.4	Analytic Results.	18
3.3	Damage modeling	19
4	Atmospheric Effects	21
4.1	Extinction	22

4.2	Optical Turbulence	24
4.3	Thermal Blooming	25
4.4	Databases and Models.	26
5	Description of Simulations	27
5.1	ANCHOR Equations.	27
5.2	Simulated Situation	28
5.2.1	Surface Platform Engagement.	28
5.2.2	Unmanned Aerial Vehicle (UAV) Engagement.	29
5.2.3	Target materials.	29
5.2.4	Atmospheric conditions	31
6	Simulations Results	35
6.1	Surface Platform.	35
6.1.1	Irradiance	35
6.1.2	Power in the Bucket	35
6.1.3	Melt Depth	36
6.1.4	Dwell Time	37
6.2	Unmanned Aerial Vehicle (UAV) Platform	41
6.2.1	Irradiance	41
6.2.2	Power in the Bucket	41
6.2.3	Melt Depth	41
6.2.4	Dwell Time	44
7	Conclusions	47
	List of References	47
	Initial Distribution List	51

List of Figures

1.1	Peru: Maritime, Amazonian, Andean, Bi-Oceanic and with Antarctic presence country.	3
1.2	Comparison between estimated cocaine production (orange bars) and seizures (blue bars) in Peru between 1994 and 2014.	4
2.1	Aluminum sheet, 3 mm thick.	11
3.1	Temperature versus depth at different dwell times for aluminum at a peak irradiance of 100 MW/m ²	15
3.2	One-dimensional geometry of laser induced melting.	16
3.3	Temperature versus depth at different dwell times for aluminum at a peak irradiance 100 MW/m ² of including melting effects.	19
3.4	Melt depths evolution of aluminum at a peak irradiance of 100 MW/m ²	20
3.5	Melt depth of aluminum versus peak irradiance at 10 seconds dwell time . . .	20
4.1	Percentage composition of the Earth's atmosphere. Other components present in minimal quantities. Water vapor is highly variable.	21
4.2	Extinction coefficient versus wavelength calculated with and without aerosols.	22
4.3	Molecular atmospheric absorption vs. wavelength.	23
4.4	Total percentage of radiation absorbed by the different components of the atmosphere at different wavelengths.	24

4.5	Hufnagel Valley Turbulence Model.	25
5.1	Peruvian Coastguard Ship Rio Pativilca.	29
5.2	Unmanned Aerial Vehicle (UAV) reference concept.	30
5.3	Reference image of the simulated target.	30
5.4	YAMAHA® V8 Offshore model F350.	32
6.1	ANCHOR results for irradiance versus cross range to the target, for various laser output powers fired from a surface platform.	36
6.2	ANCHOR results for power in the bucket versus cross range to the target, for various laser output powers fired from a surface platform.	37
6.3	ANCHOR results for melt depth versus cross range at a dwell time of 1 second from a surface platform.	38
6.4	ANCHOR results for required dwell time to melt through a 5 mm thick rubber target versus cross range from a surface platform.	39
6.5	ANCHOR results for required dwell time to melt through a 2 mm thick fiber-glass target versus cross range from a surface platform.	40
6.6	ANCHOR results for required dwell time to melt through a 3 cm thick metallic target versus cross range from a surface platform.	40
6.7	ANCHOR results for irradiance versus cross range to the target, for various laser output powers fired from a UAV platform.	42
6.8	ANCHOR results for power in the bucket versus cross range to the target, for various laser output powers fired from a UAV platform.	42
6.9	ANCHOR results for melt depth versus cross range at a dwell time of 1 second from a UAV platform.	43

6.10	ANCHOR results for required dwell time to melt through a 5 mm thick rubber target versus cross range from a UAV platform.	44
6.11	ANCHOR results for required dwell time to melt through a 2 mm thick fiber-glass target versus cross range from a UAV platform.	45
6.12	ANCHOR results for required dwell time to melt through a 3 cm thick metallic target versus cross range from a UAV platform.	45

THIS PAGE INTENTIONALLY LEFT BLANK

List of Tables

2.1	Laser classifications according to their output power	8
2.2	Advantages and limitations of laser weapons	9
5.1	Simulated HEL weapons parameters summary.	31
5.2	Target material parameters	33

THIS PAGE INTENTIONALLY LEFT BLANK

Acknowledgments

First of all, I would like to thank the Peruvian Navy for giving me the opportunity to study at NPS. Also, to Professors Keith Cohn and Joseph Blau, my advisers, for all the support, guidance and work they have put into this thesis research.

Second, I want to thank to the excellent group of officers from my cohort who were always there to encourage and help me along the past two years and to the members of the Directed Energy research group for all the feedback provided to this thesis.

Finally, my most special appreciation to Annie, my wife, who showed herself very supportive and encouraging along this long path.

THIS PAGE INTENTIONALLY LEFT BLANK

CHAPTER ONE

Introduction to Peruvian Navy Operations

1.1 Peruvian Navy History

The territory we now call Peru has a naval tradition that goes back many centuries. The earliest native people used to live from the sea through fishing and trading. They developed a civilization that eventually became part of the Inca Empire, the largest empire in the pre-Columbian era; during the fifteenth century, an Inca Empire governor named Tupac Yupanqui made a voyage to Oceania, a trip of approximately 4300 nautical miles.

After the conquest of the Inca and other native peoples by Spain in the sixteenth century, the viceroy of Peru became the most powerful enclave of the Spanish empire because it possessed the largest reserves of precious minerals. In order to protect such riches and trade, the Spanish created in 1580 the Navy of the South Sea with its headquarters located in Lima, the location of the viceroy and current capital of Peru.

In the nineteenth century, some of the officers who served in the Navy of the South Sea rebelled against the Spanish crown and fought for Peruvian independence under the command of British officers who were in the service of the independence cause. The Peruvian Navy, as it is today, was officially founded on October 8, 1821, the very same year as the independence of the country.

From the beginning, the Peruvian Navy has been involved in the conflicts that reaffirmed the independence of Peru and defined the borders with its neighboring countries. The most significant conflict was fought against Chile between 1879 and 1883. After signing the peace treaties of this war, the Peruvian government started the re-assembly of the

armed forces. To assist with this, they hired military personnel from various countries. The first contingent came from France and operated in Peru during the 1900s and 1910s. Then, another contingent arrived from the United States of America; during its operation in the 1920s and 1930s, they helped with the organization of the Peruvian Navy as we know it today.

During the second half of the twentieth century, Peru engaged in two conflicts against Ecuador due to territorial disagreements. However, one of the largest recent conflicts occurred during the 1990s. A terrorist group harboring communist ideas was operating all over the country. The Peruvian Navy had the mission of pacifying the rivers on the jungle; this task is still ongoing.

1.2 Peruvian Navy Today

Today, the Peruvian Navy has a domain shown in Figure 1.1. Its official mission is to “exert the surveillance and protection of the national interests in the maritime, river and lake areas; and support the nation’s foreign policies through naval power; contribute to the control of the internal order; help with the economic and social development of the country and participate in civil defense activities, according with the law; in order to contribute to the guarantee of the independence, sovereignty and territorial integrity of the Republic and wellness of the population in general” [1].

1.3 Peruvian Navy Responsibilities

Besides normal defense activities, the Peruvian Navy has to deal with several illicit activities occurring within its jurisdiction. These activities are illegal logging, mining, fishing, and drug trafficking.

Illegal logging occurs in the Amazon area; this activity is responsible for thousands of acres of deforestation, which affects the environment and endangers the native species. After wood is cut, it is transported using the rivers that flow through the area.

Illegal mining also occurs in the Amazon area; this activity takes place on the riversides and involves treating the mineral sediments carried by the rivers from the Andes Mountains. The harsh chemicals used for this treatment are later dumped into the rivers, which



FIGURE 1.1 Peru: Maritime, Amazonian, Andean, Bi-Oceanic and with Antarctic presence country. Adapted from [1].

contaminate all the surrounding areas downstream, destroying the Amazon ecosystem on its way.

Illegal fishing takes place in the Pacific Ocean, where entire fleets of fishing ships, which come mainly from Asia, catch fish from Peru's maritime domain and take them to big factory ships outside the country's jurisdiction. Besides not having fishing permits, these vessels violate Peruvian law prohibiting the fishing of certain species during their reproduction and growing season, affecting the conservation of marine life.

Drug trafficking is probably the most threatening of the illegal activities the Peruvian Navy must address, not only because of the damage these products cause to consumers around the world, but because the profits generated allow the producers to hire their own militia groups to defend themselves. These militias consist mostly of the remnants of terrorist groups with communist ideologies that used to operate in the 1980s and 1990s. A cocaine run out of Peru starts in the Andes region, where it is produced and taken by land to one of the Amazon rivers or to the coast. Once there, it is loaded on small watercrafts, equipped

with big outboard motors, and taken to larger vessels. In this way, they avoid customs inspections, and their speed makes them hard to catch.

The indicator used for cocaine production by the United Nations in the World Drug Report is the “potential production,” which is calculated as a function of the coca leaf crop area available by country. The latest report was given in 2016 and it shows this indicator from 1994 to 2014.

Figure 1.2 shows the estimated amount of cocaine produced (orange bars), according to the potential production indicator reported by the United Nations Office on Drugs and Crime (UNODC) in the 2016 World Drug Report; the blue bars indicate the amount of cocaine seized by Peruvian authorities reported to the UNODC on the Annual Drugs Report Questionnaire database. This graph shows that only a small fraction of the overall production is seized in Peru each year, and indicates the magnitude of the task required of the Peruvian Navy for drug interdiction.

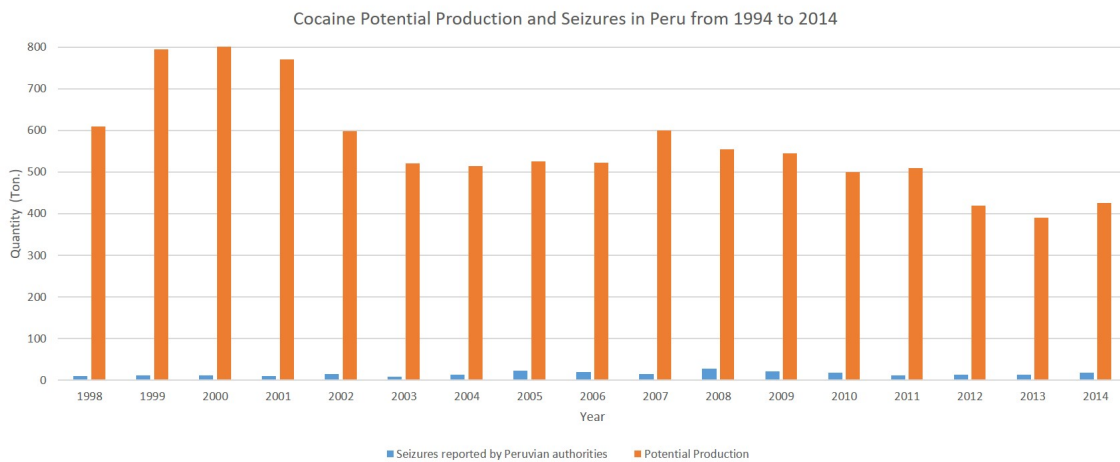


FIGURE 1.2 Comparison between estimated cocaine production (orange bars) and seizures (blue bars) in Peru between 1994 and 2014. Adapted from [2].

1.4 Motivation for Directed Energy Employment for Interdiction

Interdiction is defined by the Oxford dictionary as “the action of intercepting and preventing the movement of a prohibited commodity or person.” Thus, in order to have a successful

lawful interdiction, it is necessary to capture the commodities that are trafficked and the people handling them. Since Peru is a signatory country of the American Convention on Human Rights "Pact of San Jose, Costa Rica", it is paramount to seize the illegal cargo, and people carrying it without damage. This is why directed energy weapons might be helpful for interdiction since they may be able to disable the crafts used to transport the commodities with great precision, from a safe distance without harm to persons and cargo.

THIS PAGE INTENTIONALLY LEFT BLANK

CHAPTER TWO

Directed Energy Overview

If we take a brief look at the evolution of warfare, we can see that technological advances in weaponry (from the arrow to the ballistic missile) have evolved towards better range, accuracy and precision. Most conventional weapons use a projectile to deliver an impact or explosive to the target.

For a long time, people have wondered about the possibility of delivering focused, nearly instantaneous energy to a target. Examples of this concept can be traced to ancient times, when Archimedes is said to have used mirrors to focus sunlight to burn ships that were attacking Syracuse. In more recent times, science-fiction literature and movies have introduced directed energy weapons in their stories.

2.1 Introduction to Directed Energy

There are several types of directed energy weapons, but in this study we will discuss only high-energy lasers. The term “laser” is an acronym that stands for “light amplification by stimulated emission of radiation”. Einstein introduced the theory in the early 1900’s, and the technology was developed during the second half of the twentieth century. The first prototype was a microwave laser (maser), made in 1954 by Charles Townes, with funding by the U.S. Office of Naval Research. In the following years, various agencies developed their own technology and made multiple different kinds of lasers.

Most lasers have the following three common components:

1. Pumping source: Provides the energy to excite the gain medium and start the lasing process. It can be another light source or an electrical or chemical reaction.
2. Gain medium: Amplifies the laser light. It can be a solid, gas, plasma, or liquid.

3. Optical cavity: Stores the laser light, allowing it to grow over many passes through the gain medium. It typically consists of a highly reflecting mirror at one end, and a partially reflecting mirror at the other end, which allows some of the coherent laser light to be transmitted to the application.

According to their average output power, lasers are designated by four different classes, as listed in Table 2.1.

TABLE 2.1 Laser classifications according to their output power [3].

Class	Denomination	Comments
1	Low power (< 0.5 mW)	Not for weapons use. Example: Bar code reader.
2	Moderate power (< 1 mW)	Not for weapon use. Example: Laser pointers.
3	Medium power (< 500 mW)	Not for weapon use. Example: Laboratory lasers.
4	High power (> 500 mW)	Used for industry, medicine, and for weapons.

High-energy lasers have several advantages and limitations. Table 2.2 presents a comparison between those.

The applications of high-energy lasers for naval purposes depend on the output power. Lasers with an output power on the order of tens of kilowatts can be effective against slow moving targets, small aircraft, drones, or watercraft, and can be used to blind or disable sensors (“soft kill”), disable motors or detonate explosives. On the other hand, lasers with an output power on the order of hundreds of kilowatts to megawatts can be used for “hard kills” of high-speed missiles and larger aircraft.

2.2 High Energy Lasers Classification

The first technology to reach an output power on the order of hundreds of kW in the 1960s was a gas dynamic laser. This laser uses a combustion chamber to generate gas at high temperature and pressure. This gas is then passed through a nozzle to excite the gain medium where it generates a laser beam with a wavelength of approximately 10.6 μm . Its

TABLE 2.2 Advantages and limitations of laser weapons [3].

Advantages	Limitations
A laser can deliver payloads up to the order of MJ of energy with great precision at long distances, with minimum collateral damage.	Since the laser beam travels in a straight line, range is limited by the line of sight of the weapon.
Energy is delivered at the speed of light, thus reducing maneuver opportunities by the target.	Damage is cumulative, so the laser beam needs to dwell on the target for some time (up to ~10 sec) to destroy or disable it.
By adjusting the output power, it can be adapted to deliver the desired type or level of damage.	Its performance can be affected by weather and atmospheric conditions.
It can fire as many times as the energy storage of the platform allows.	It is sensitive to countermeasures such as a reflecting or rotating target.
The cost per shot is approximately \$1 (cost to produce the input energy)	The production and implementation can be expensive and large.
It does not involve the use of any explosive, so it is safer to handle and operate.	There can be collateral damage to friendly aircraft or satellites operating in the same area.

advantages are that it generates a good quality beam, with a relatively high power, and the technology is already mature. However, its magazine is limited by the gas supply, and the wavelength obtained is not good for propagation in the maritime environment, which makes it a poor option for naval purposes [3].

A chemical laser first reached the MW output power level in the 1970s. This technology mixes chemicals in supersonic nozzles and uses the products of the chemical reactions to excite the gain medium. One type is a deuterium-fluoride (DF) laser, which produces a beam with a wavelength of approximately 4 μm . Another type is a chemical oxygen-iodine (COIL), which produces a laser beam with a wavelength of approximately 1.3 μm . This technology is also mature and generates a laser beam of good quality at high power, and its shorter wavelengths are better than the gas laser for atmospheric propagation. However,

its magazine is also limited by the supply of chemical reactants, and the exhaust chemicals are highly toxic, so it is also a poor option for naval purposes [3].

Another technology that has become very popular is the solid state laser (SSL). It uses a rod, slab, or fiber substrate embedded with a dopant such as Nd or Yb as the gain medium. It is pumped by an external source of light, such as a flash lamp or diodes, and it typically produces a laser beam with a wavelength of approximately 1 μm , which is good for atmospheric propagation. This kind of laser has the advantage of being compact and light weight; also, it does not use any harmful chemicals or gases, and it can reach a high output power with a relatively good efficiency. Another advantage is that it is powered by the ship's electrical system, so the magazine is only limited by available ship power and energy storage. One disadvantage is that the fixed substrate in the gain medium has low thermal conductivity, which limits the output power to the order of tens to possibly hundreds of KW. Achieving higher output power generally requires combining multiple SSL beams, which tends to reduce the output beam quality [3].

A less conventional technology is the free electron laser (FEL). It uses a particle accelerator to accelerate free electrons to relativistic speeds. The electron beam then passes through an undulator (a series of alternating magnets) to create and amplify coherent light. One of the advantages it offers are tunability, which means that the operator can chose the most suitable wavelength for the current tactical situation. Another advantage is that since there is no fixed gain medium, it can scale to higher power levels, potentially reaching the order of MW. It also offers an excellent beam quality for long distance propagation, and its size and complexity do not scale with output power. Nevertheless, this technology is not yet as mature as other laser types, it requires a larger and heavier set up, and shielding from radiation produced by the relativistic electrons is needed [3].

2.3 Laser Weapon Performance Metrics

A laser weapon operates by focusing a beam of light onto a target for a finite period of time. The damage to a target depends on the power of the laser, the amount of time it spends on the same aim spot, and the target's composition. The performance of a laser can be quantified by several values; for this study, we will use three of them: irradiance, power in the bucket, and dwell time.

2.3.1 Irradiance

Irradiance is the power (P) a laser delivers to its target divided by the beam area (A), and has units of power per area [4]:

$$I = \frac{P}{A}. \quad (2.1)$$

2.3.2 Power in the Bucket

Another parameter we will use in this study is the power-in-the-bucket. The “bucket” is defined as the area on the target we wish to damage. This “power-in-the-bucket” is how much laser power fills within this designated target area [5]. Figure 2.1 shows graphically an example of how the “bucket” is defined; in this case the target is a 3 mm thick aluminum sheet with a bucket diameter of 10 cm.

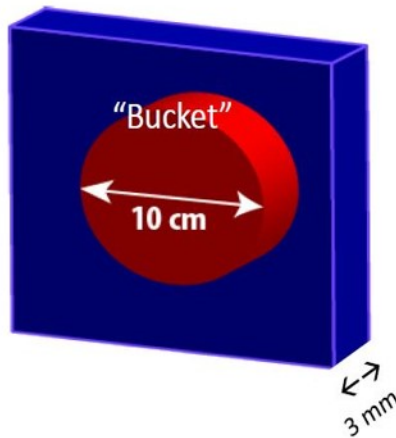


FIGURE 2.1 Aluminum sheet, 3 mm thick, with a 10 cm diameter bucket. Source: [5].

2.3.3 Dwell Time

The dwell time is the time an HEL is needs to remain in the target to affect the appropriate damage. In this study we will specifically look for the dwell times required to melt through materials of different thicknesses.

THIS PAGE INTENTIONALLY LEFT BLANK

Target Damage Physics

The energy provided by a high energy laser (HEL) weapon that is absorbed by a target causes a change in the target's temperature, which can eventually lead to its melting. However, not all the energy delivered by the laser weapon produces that effect; some of the energy will be conducted or radiated away by the target materials, depending on their physical characteristics. In this study, we want to estimate how long it takes to melt through a material to a certain depth.

3.1 Laser Heating of Materials and Conductive Losses

When a material is heated by an HEL, it conducts the energy away from the laser spot to the cooler regions of the material based upon its physical properties. These conductive losses must be taken into account when calculating the power to be deposited into a target to cause damage. This conduction mechanism is described by the following heat-flow equation [6]:

$$\frac{dT(\vec{r}, t)}{dt} = \frac{k}{\rho c_p} \nabla^2 T + \frac{S(\vec{r})}{\rho c_p}, \quad (3.1)$$

where $T(\vec{r}, t)$ is the temperature function, k is the thermal conductivity of the material, ρ is the density of the material, c_p is the specific heat of the material, $S(\vec{r})$ is the source term (power input per unit volume provided by the laser weapon), and $\nabla^2 T$ is the Laplacian of the temperature. This equation does not consider the melting of the material and it assumes that material properties (k , ρ , and c_p) are constant (independent of position and time).

The source term is a function of the irradiance delivered to the target and takes into account its optical absorption coefficient and its reflectance. Since the laser beam is absorbed within the first few nanometers for a metallic target, we will assume the source term to be non-zero

only at the surface ($x = 0$) according to [6]:

$$S(x) = \begin{cases} \alpha I(1 - R) & x = 0 \\ 0 & x > 0, \end{cases} \quad (3.2)$$

where α is the optical absorption coefficient of the material, I is the peak irradiance delivered by the HEL, and R is the fraction of the optical power that is reflected by the target. Here it is assumed that the shape of the laser spot at the target has a uniform (“flat - top”) profile.

In order to have a sense of how the conductive mechanism diffuses heat away, we can evaluate the heat diffusion equation for a one-dimensional case (where the x -direction is into the target) and assuming a semi-infinite slab of material. The analytic solution for the heat flow equation in 1-D is given by [6]:

$$T(x, t) = T_0 + \frac{2I(1 - R)}{k} \sqrt{Dt} \operatorname{ierfc} \left[\frac{x}{2\sqrt{Dt}} \right], \quad (3.3)$$

where t is the time, $D = k/(\rho c_p)$ is the thermal diffusivity of the material, and T_0 is the ambient temperature. The integrated complementary error function is given by [6]:

$$\operatorname{ierfc}(x) = \int_x^{\infty} \operatorname{erfc}(\xi) d\xi,$$

with

$$\operatorname{erfc}(x) = 1 - \operatorname{erf}(x) = 1 - \frac{2}{\sqrt{\pi}} \int_0^x e^{-t^2} dx,$$

This 1-D approach is a good approximation for the material at the center of the laser spot so long as the laser spot is much larger than the diffusion length. As an example, using the material parameters for aluminum ($k = 226 \text{ W}/(\text{m} \cdot \text{K})$, $\rho = 2700 \text{ kg}/\text{m}^3$, $c_p = 864.7 \text{ J}/(\text{kg} \cdot \text{K})$ [7] and, $\alpha \approx 0.1 \text{ nm}^{-1}$ [8]), a peak irradiance $I = 100 \text{ MW}/\text{m}^2$, and an ambient temperature of $T_0 = 300 \text{ K}$, we obtain the results shown in Figure 3.1. We can

see the temperature profile at different dwell times follows an approximately exponential profile. These results are not physically realistic, because the profile does not change when it crosses the melting temperature.

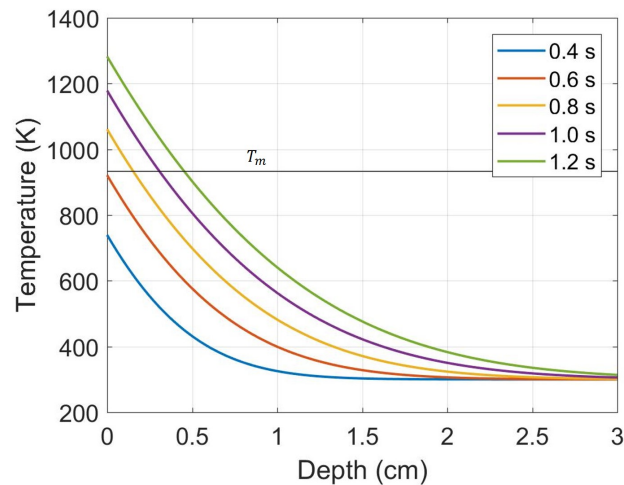


FIGURE 3.1 Temperature versus depth at different dwell times for aluminum at a peak irradiance of 100 MW/m^2 . The horizontal black line indicates the melting temperature of aluminum.

3.2 Laser Induced Melting

The previous section did not include melting, but established that the temperature profile is approximately exponential and that the surface reaches melting temperature rapidly. The goal of this section is to develop a model of melt depth versus dwell time.

The process of laser induced melting does not happen instantaneously; the absorbed energy first heats the surface and the heat is conducted away into the material. During the time the laser is on, this results in the existence of two defined regions within the material with their own physical properties and temperature profiles. The region closest to the surface reaches its melting point faster and becomes liquid while the region deeper into the material remains solid; a diagram of this geometry is shown in Figure 3.2, where the x -axis is the depth within the material, with surface is at the origin, and the interface between the liquid and solid regions is given by $X(t)$.

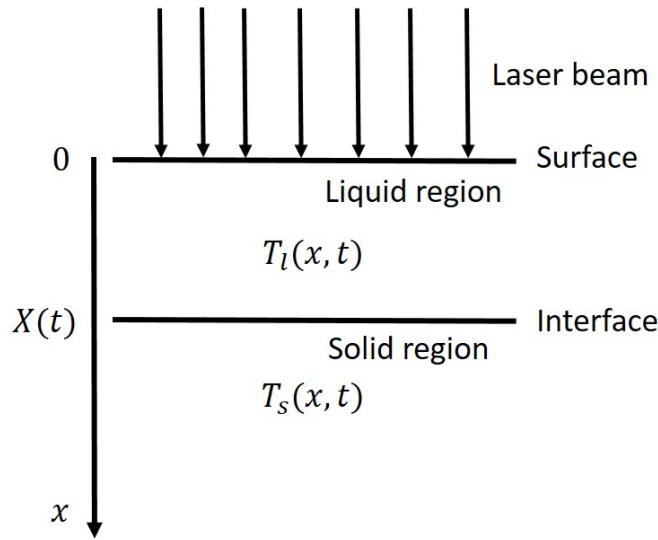


FIGURE 3.2 One-dimensional geometry of laser induced melting. Adapted from [8].

3.2.1 Assumptions

The interaction between laser radiation and the target materials is a complicated process that has been extensively studied and modeled. One of the approaches to describe these interactions is by making a one-dimensional mathematical model assuming [8]:

1. A semi-infinite slab of material whose physical properties do not change with the increase in the temperature, for a given phase (solid or liquid).
2. Different phases can have different properties.
3. The melted material stays in the same place.

3.2.2 Real Life Effects

Even though the assumptions presented in the previous section make it easier to obtain analytical results for the heat flow equation, the effects in real life could be quite different. There are several ways that reality departs from our assumptions:

1. The target materials have a finite depth; thus, heat cannot be conducted to infinity. Also, air is very likely to be at the other end of the material; which acts as a better

insulator compared with metallic materials. These effects may lead to shorter dwell times because the heat gets better confined within the material.

2. The heat flows in three dimensions, spreading in all directions into the material. This may lead to longer dwell times. This effect becomes especially important when the laser spot size is much smaller than the material depth, which mainly occurs at shorter ranges.
3. The melted material is likely to be cleared away (by gravity or wind), making new regions of the material exposed to direct heating. This may lead to shorter dwell times.

For the longer ranges, where the spot size is longer than the melt depth, we can ignore the 3-D effects. Thus, the dwell times for longer ranges will probably be overestimated using this approach. For shorter ranges, the 3-D effects may lead to underestimates of the dwell times using this approach, but dwell times for the shorter ranges are already relatively small. Any modest increase in the dwell times at shorter ranges will have minimal impact on operational performance.

3.2.3 Boundary Conditions

In order to solve the heat flow equation for each of the regions formed during the melting process, we need to consider the following boundary conditions [7]:

1. The temperature at the liquid-solid interface $X(t)$ is equal to the melting temperature T_m of the material, $T_l = T_s = T_m$ at $x = X(t)$.
2. The temperature of the solid region T_s is equal to the ambient temperature T_0 when:
 - (a) The dwell time t is equal to zero, $T_s = T_0$ at $t = 0$.
 - (b) The distance x into the material goes to infinity, $T_s = T_0$ as $x \rightarrow \infty$.
3. The liquid-solid interface at time zero is $X(t = 0) = 0$.
4. Energy is conserved across the boundary,

$$k_l \frac{\partial T_l(x, t)}{\partial x} = k_s \frac{\partial T_s(x, t)}{\partial x} - \rho L \frac{dX(t)}{dt}, \quad (3.4)$$

where L is the latent heat of fusion of the material.

3.2.4 Analytic Results

Using a one-dimensional approach to solve the heat-flow equation, we can obtain analytical solutions for the temperature as a function of position and time for the liquid (subscript l) and solid (subscript s) regions formed during the melting process that satisfy the boundary conditions.

Liquid region

The temperature profile in the liquid region ($0 \leq x \leq X(t)$) is assumed to be [7]:

$$T_l(x, t) = T_m - \frac{AI}{k_l} [x - X(t)] + \frac{AI}{2D_l k_l \left[1 + \frac{X(t)}{D_l} \frac{dX(t)}{dt} \right]} \times \frac{dX(t)}{dt} [x^2 - X^2(t)], \quad (3.5)$$

where A is the absorptivity of the material and D is the thermal diffusivity of the material.

Solid region

The temperature profile in the solid region ($X(t) \leq x \leq \infty$) is assumed to be [7]:

$$T_s(x, t) = T_m - (T_m - T_0) \left\{ 1 - \exp \left[-\frac{1}{D_s} \frac{dX(t)}{dt} (x - X(t)) \right] \right\}. \quad (3.6)$$

Liquid-solid interface

The liquid-solid interface $X(t)$ position represents the melt depth as a function of time. Using the above temperature profiles, the solution to 3.4 is [7]:

$$X(t) = \left[-\frac{b_0}{2} + \left(\frac{b_0^2}{4} + \frac{a_0^3}{27} \right)^{1/2} \right]^{1/3} + \left[-\frac{b_0}{2} - \left(\frac{b_0^2}{4} + \frac{a_0^3}{27} \right)^{1/2} \right]^{1/3} - \frac{D_l m_s}{16AI}, \quad (3.7)$$

with

$$m_s = \rho [c_p (T_m - T_0) + L],$$

$$a_0 = \frac{3D_l^2 m_s^2}{256(AI)^2} \left(\frac{192(AI)^2 t}{D_l m_s^2} + 31 \right), \text{ and}$$

$$b_0 = -\frac{D_l}{8AI} \left[\frac{D_l^2 m_s^3}{256(AI)^2} \left(\frac{288A^2 I^2 t}{D_l m_s^2} + 47 \right) + \frac{t(18A^2 I^2 t + 3D_l m_s^2)}{m_s} \right].$$

Using the same conditions shown in Figure 3.1 we can plot the results for the heat flow equation taking into account the melt effects. These results are shown in Figure 3.3. Here we observe how the melting affects the temperature profile by producing a kink at the melting temperature; this kink represents the melt front at different dwell times. Also, the temperature at the surface for the different dwell times is noticeably higher than in the previous situation because, in the liquid state, the thermal conductivity decreases significantly compared to the solid state [7].

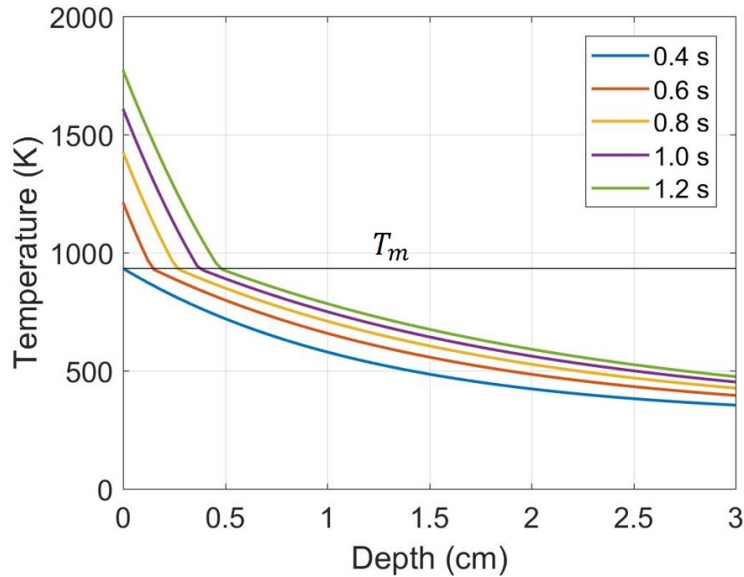


FIGURE 3.3 Temperature versus depth at different dwell times for aluminum at a peak irradiance of 100 MW/m^2 , including melting effects. The horizontal black line indicates the melting temperature of aluminum.

3.3 Damage modeling

In order to get a feel for how the melt depth evolves, we can use the equations from section 3.2 to plot different results using the material parameters for aluminum. In Figure 3.4 we see the melt depth for a peak irradiance of 100 MW/m^2 up to a dwell time of 10 seconds.

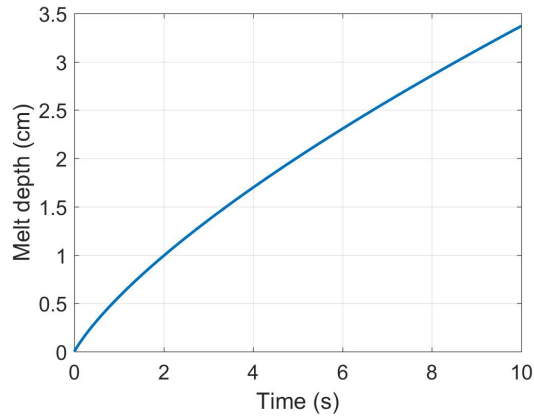


FIGURE 3.4 Melt depths evolution of aluminum at a peak irradiance of 100 MW/m^2

Figure 3.5 shows the different melt depths reached on aluminum at a dwell time of 10 seconds for peak irradiances going from 10 MW/m^2 to 1 GW/m^2 .

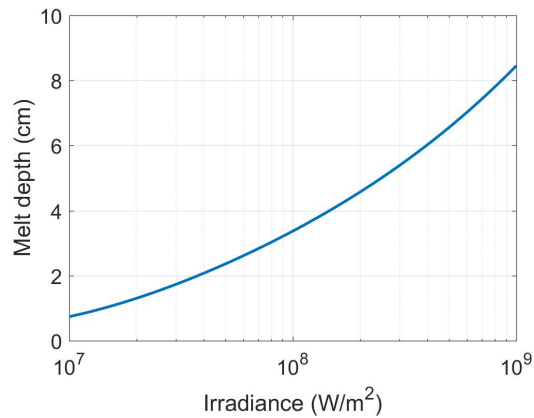


FIGURE 3.5 Melt depth of aluminum versus peak irradiance at 10 seconds dwell time

This damage formulation will be of great utility for this study because it will help estimate the dwell times needed to cause the desired damage to a target using the irradiances delivered by the laser weapons to be simulated.

CHAPTER FOUR

Atmospheric Effects

A laser beam has to travel the distance between the weapon and the target through the atmosphere and is subject to different losses of energy along this path. It is critical to take these losses into account because they will determine the output power required for a laser weapon to deliver the irradiance needed to make the target non-operational.

The atmosphere is composed of different gas molecules of various types and concentrations. The main components of the Earth's atmosphere are shown in Figure 4.1 . These components have their own physical characteristics that can cause effects such as extinction, turbulence, and thermal blooming.

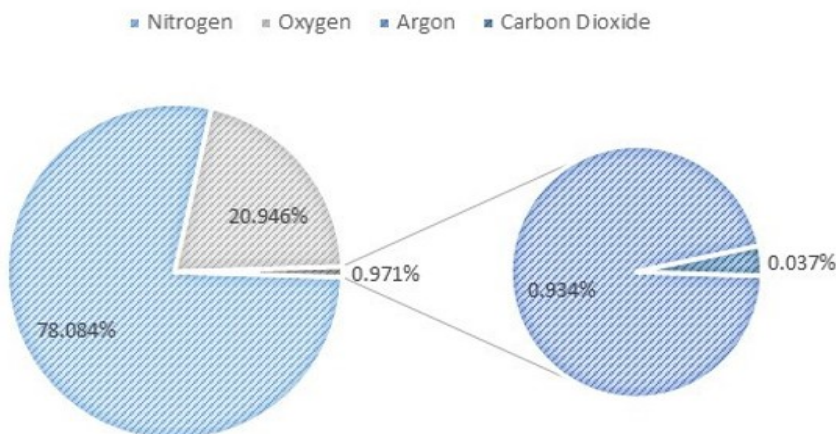


FIGURE 4.1 Percentage composition of the Earth's atmosphere. Other components present in minimal quantities. Water vapor is highly variable. Adapted from [9].

4.1 Extinction

Extinction is the loss of power of the laser beam during its transit to the target. It is caused by the presence of molecules and aerosols in the atmosphere. They cause two different effects: absorption and scattering. Beer's law describes extinction effects on the output power of a laser [10]:

$$P(z) = P_0 e^{-\epsilon z}, \quad (4.1)$$

where P_0 is the output power at the beam director, z is the range to the target, $P(z)$ is the power delivered at distance z , and ϵ is the extinction coefficient.

The extinction coefficient ϵ is the sum of the contributions from the absorption (α) and scattering (β) coefficients of the molecules (subscript m) and aerosols (subscript a) present in the atmosphere [10]:

$$\epsilon = \alpha_m + \alpha_a + \beta_m + \beta_a. \quad (4.2)$$

It is important to take in account coefficients from both molecules and aerosols because, as shown in Figure 4.2, there is a dramatic difference between the extinction coefficients calculated with and without aerosols.

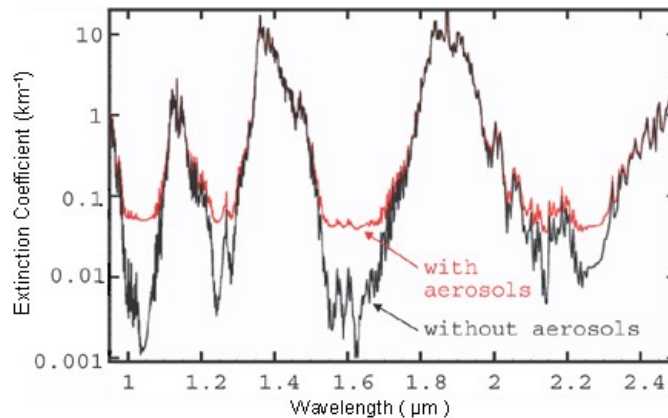


FIGURE 4.2 Extinction coefficient versus wavelength calculated with and without aerosols. Source: [11].

Molecular atmospheric absorption happens when the energy delivered from the laser beam excites the molecules in the air. This form of excitation for molecules goes into rotational and vibrational transitions that ultimately produce heat. The coefficient α_m can

be calculated from quantum theory or measured experimentally. Figure 4.3 shows the values for α_m for a tropical atmosphere at sea level, over a range of wavelengths.

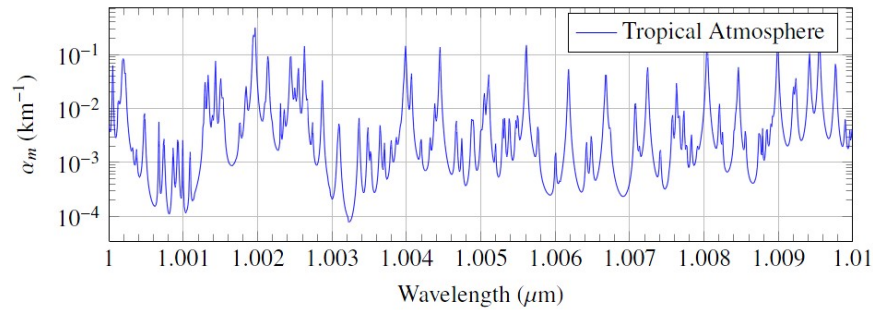


FIGURE 4.3 Molecular atmospheric absorption versus wavelength. Source: [3].

The aerosol absorption and scattering coefficients (α_a and β_a) can be determined using Mie scattering theory. This theory assumes that the scattering particle is spherical, has a single refractive index, and the incident field is a plane wave. All of these assumptions allow calculations of the scattered field at a certain angle and distance from the particle.

Molecular atmospheric scattering happens when the laser beam hits molecules in the atmosphere and, instead of being absorbed, it is deflected in different directions. The molecular scattering coefficient (β_m) can be determined using the Rayleigh scattering approximation. This approximation is used since the molecules have a radius much smaller than the wavelength of the laser beam. For Rayleigh scattering, shorter wavelengths scatter more. For example, the sky appears to be blue during the daytime because the components of the atmosphere scatter light in the blue part of the spectrum (between 450 and 495 nm) more efficiently than red light.

Figure 4.4 shows the total percentage of radiation absorbed by the atmosphere according to its wavelength for its different components. There, we appreciate the “transparency windows,” which are wavelengths at which most radiation will pass with less absorption and scattering, such as $1 \mu\text{m}$, $1.6 \mu\text{m}$, $2.1 \mu\text{m}$, $4 \mu\text{m}$, etc.

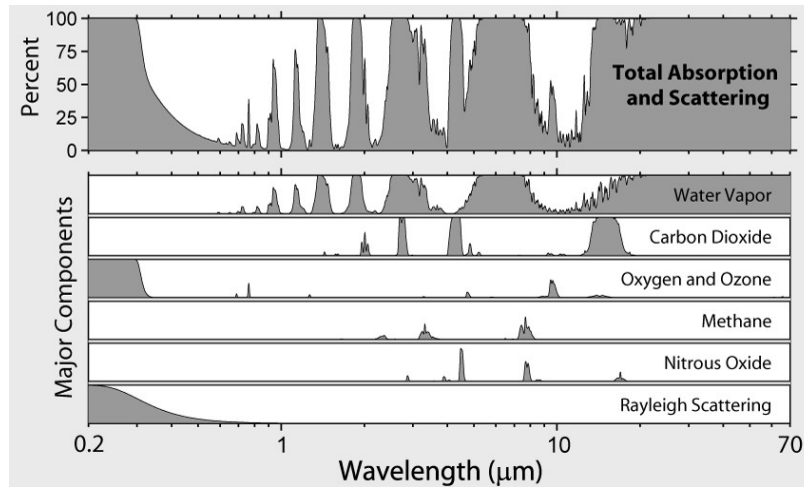


FIGURE 4.4 Total percentage of radiation absorbed by the different components of the atmosphere at different wavelengths. Source: [3].

4.2 Optical Turbulence

Turbulence is related to random heating and motion of molecules in the atmosphere, resulting in random fluctuations of the air density due to temperature and humidity variations. This leads to random variations in the refractive index of the atmosphere along the beam path. Consequently, the rays of the laser are perturbed, causing the time-averaged laser spot to become larger. These effects are especially prominent in the surface layer. Turbulence effects can be quantified by the refractive structure constant (C_n^2) and by the Fried parameter (r_0).

The refractive structure constant (C_n^2) has units of $\text{m}^{-2/3}$ and was parametrized theoretically by the Soviet mathematician Andrey Komogorov in the 1940s. This parameter describes the severity of turbulence; a larger C_n^2 value means stronger turbulence. The C_n^2 value varies as a function of altitude, and it tends to decrease with altitude near the surface, as shown in Figure 4.5. Typical values for the refractive structure constant are approximately $10^{-17} \text{ m}^{-2/3}$ for weak turbulence and $10^{-13} \text{ m}^{-2/3}$ for strong turbulence [10].

The Fried parameter (r_0) has units of length (m) and is defined as the diameter over which the beam maintains transverse coherence throughout the propagation length. As turbulence grows stronger, the laser beam is not able to keep its coherence across its

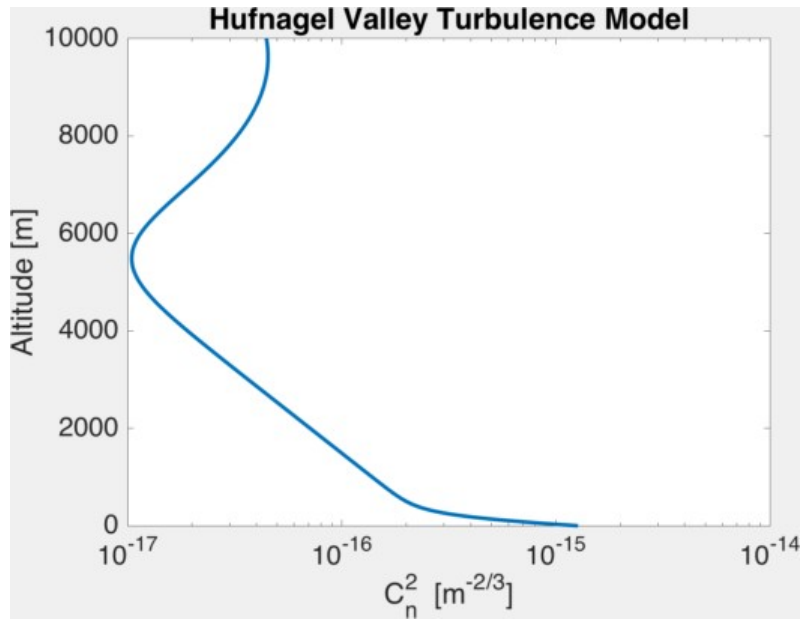


FIGURE 4.5 Hufnagel Valley Turbulence Model. Source: [3].

original diameter; thus, the Fried parameter gets smaller for stronger turbulence. When r_0 becomes less than the beam director diameter, the laser beam will be strongly affected by the turbulence and spread out. If the C_n^2 number is constant, the Fried parameter becomes [10]:

$$r_0 \approx 0.33 \frac{\lambda^{6/5}}{R^{3/5} (C_n^2)^{3/5}}, \quad (4.3)$$

where λ is the wavelength of the laser beam and R is the range to the target.

4.3 Thermal Blooming

Thermal blooming happens because of atmospheric absorption. The air molecules increase their temperature as they absorb energy, which changes the air density and hence the index of refraction of the air. These changes make the region act as a lens that de-focuses the laser beam, causing it to spread. Wind also affects the laser beam since it cools down the air column where the beam is traveling, making the beam steer into the wind. Thermal blooming is un-avoidable at high output powers but can be somewhat mitigated by selecting techniques such as emitting in a wavelength that reduces absorption.

4.4 Databases and Models

All the atmospheric effects mentioned before have been widely studied over the years and now there are several databases and models to calculate them. We present some of these on the following list.

- HITRAN. This acronym stands for High Resolution Transmission. It is a database of transmission spectra for approximately 50 molecular species. It is maintained by the Harvard-Smithsonian Center for Astrophysics and is used as data source for multiple atmospheric propagation codes. [3]
- MODTRAN. This acronym stands for Moderate Resolution Transmission. It is a radiative transfer code that calculates the transference of electromagnetic radiation through the atmosphere using HITRAN database and taking into account pre-calculated absorption and scattering coefficients for different atmospheric conditions. [3]
- LEEDR. This acronym stands for Laser Environmental Effects Definition & Reference. It is developed by the AFIT Center for Directed Energy. This model creates profiles of temperature, pressure, water vapor, particulate content, turbulence, and other parameters versus altitude for a determined location and time by predicting the atmospheric conditions based on historical data. [3]
- COAMPS. This acronym stands for Coupled Ocean Atmosphere Mesoscale Prediction System. It is a high resolution weather forecasting model developed by the Naval Research Laboratory at Monterey and it is used by the US Navy to forecast atmospheric conditions such as temperature, wind profiles, aerosols, etc. [3]
- NAVSlaM. This acronym stands for Navy Atmospheric Vertical Surface Layer Model. The model was developed by Paul Frederickson from the NPS Meteorology Department. It computes the vertical refractive structure constant (C_n^2) profiles over the ocean up to 100 m above the surface using the wind speed, air and sea temperatures, humidity and pressure of a region, and assuming they are steady and horizontally homogeneous. [3]

CHAPTER FIVE

Description of Simulations

The simulations in this study are performed using the ANCHOR laser performance code developed by the NPS Physics Directed Energy Group. This code uses the databases and models mentioned in the previous section to predict the time averaged irradiance on target for a given laser output. It also takes into account the effects caused by the diffraction, jitter, turbulence, thermal blooming, etc, on the laser beam, and relative motion between platform and target.

5.1 ANCHOR equations

In order to perform the calculations mentioned before, this code uses the following master equation [10]:

$$\langle I \rangle = \left(\frac{P e^{-\int \epsilon(z) dz}}{\pi w_{tot}^2} \right) S_{TB}, \quad (5.1)$$

where $\langle I \rangle$ is the time averaged irradiance, P is the laser output power, $\epsilon(z)$ is the extinction coefficient, S_{TB} is the thermal blooming Strehl ratio, and w_{tot}^2 is the spot size at the target.

The thermal blooming Strehl (S_{TB}) ratio is the relationship between the time averaged irradiance with and without thermal blooming [10]:

$$S_{TB} = \frac{\langle I \rangle_{TB}}{\langle I \rangle_{noTB}}. \quad (5.2)$$

The spot size at the target (w_{tot}^2) is the sum of the contributions from diffraction (w_d^2), jitter (w_j^2), and turbulence (w_t^2) effects [10]:

$$w_{tot}^2 = w_d^2 + w_j^2 + w_t^2. \quad (5.3)$$

The spot size at the target from the diffraction contribution (w_d) is calculated using [10]:

$$w_d = M^2 \left(\frac{2\lambda R}{\pi D} \right), \quad (5.4)$$

where M^2 (≥ 1) is the beam quality factor of the laser, R is the range to the target, D is the diameter of the laser beam at the beam director, and λ is the wavelength of the laser beam.

Jitter of the laser spot position on the target can be caused by multiple reasons such as the platform motion, tracking error, or turbulence induced beam wander. The spot size at the target from the jitter contribution (w_j) is calculated using [10]:

$$w_j = \theta_{rms} R, \quad (5.5)$$

where θ_{rms} is the angular variance due to jitter (typically on the order of μrad) and R is the range to the target.

The spot size at target from the turbulence contribution (w_t) is calculated with [10]:

$$w_t = \frac{2\lambda R}{\pi r_0}, \quad (5.6)$$

where R is the range to the target, λ is the wavelength of the laser beam and r_0 is the Fried parameter (calculated using equation 4.3 if r_0 is constant).

5.2 Simulated Situation

In this study, we will simulate two situations. In both of them, the target is a small fiberglass boat transporting a large amount of high purity cocaine. This boat is trying to deliver its cargo to a larger ship, which is waiting several miles away from the coast. The boat is going at 35 knots, being propelled by one or more outboard motors. The goal is to disable the craft without damaging its crew and cargo within the time it takes to reach the larger vessel.

5.2.1 Surface Platform Engagement

In the first situation, the outlaw watercraft is being prosecuted by a coast guard ship, like the one shown in Figure 5.1, which has a maximum speed of 30 knots; thus, it is impossible

to capture the watercraft without first disabling it. The coast guard ship is equipped with either a 10 kW, 30 kW, or 100 kW output HEL weapon and is firing at variable ranges from the target. The simulated characteristics of the HEL weapon are typical values, such as a beam quality $M^2 = 1.5$, an angular variance due to jitter of $\theta_{rms} = 5 \mu\text{rad}$ [10], a beam director diameter of 30 cm, and a lasing wavelength $\lambda = 1.064 \mu\text{m}$.



FIGURE 5.1 Peruvian Coastguard Ship “Rio Pativilca.” Source: [1].

5.2.2 Unmanned Aerial Vehicle (UAV) Engagement

In the second situation, the outlaw watercraft is being prosecuted by a coast guard unmanned aerial vehicle (UAV), a concept of such vehicle is shown in Figure 5.2, flying at an altitude of 500 meters. The UAV is traveling at a speed of 130 km/h and is equipped with either a 10 kW, 30 kW, or 50 kW output HEL weapon, and will engage the target at variable ranges. The simulated characteristics of the HEL weapon are the same as listed for the first situation with the exception of the beam director diameter, which will be set at 20 cm due to presumed space and weight limitations of the platform.

5.2.3 Target materials

Figure 5.3 shows a good example of a target watercraft. In it we can see the set up of the outboard motors and their fuel lines, which will ultimately be the targets of our HEL weapon. The best and easiest course of action to interdict the outlaw watercraft is to cut



FIGURE 5.2 Unmanned Aerial Vehicle (UAV) reference concept.
Source: [12].

the fuel supply by melting its rubber fuel lines. However, such lines must be in the line of sight with the laser weapon, as shown in Figure 5.3.

However, since this may not always be possible, we must consider the possibility of disabling its outboard motor by aiming the HEL weapon at its dome. Most outboard motors are made of aluminum or stainless steel and are covered by a dome made of a fiberglass polyester resin composite. Table 5.2 shows the parameters for each of the materials.



FIGURE 5.3 Reference image of the simulated target. Adapted from [13].

TABLE 5.1 Simulated HEL weapons parameters summary.

Parameter	Platform	
	Surface	UAV
Altitude	10 m	500 m
Output Power	10 kW, 30 kW, or 100 kW	10 kW, 30 kW, or 50 kW
Beam quality (M^2)	1.5	1.5
Variance due to jitter (θ_{rms})	5 μ rad	5 μ rad
Beam director diameter	30 cm	20 cm
Laser wavelength (λ)	1.064 μ m	1.064 μ m
Speed	30 knots	70 knots

If the fuel lines are accessible, the HEL weapon must only melt through 5 mm of rubber for each line. If not, in order to disable the motor, the HEL weapon must melt through 2 mm of the fiberglass polyester resin composite cover and through about 3 cm of metal (aluminum or stainless steel) on the motor parts, per motor.

In order to estimate the 3 cm melt distance into the engine parts, we looked at the blueprints of a YAMAHA® V8 offshore model F350 outboard motor (the largest available from this company) [14]. There we identified the sensible parts to be the cylinder head, the fuel ducts and the shaft. Figure 5.4 shows a diagram of this motor with arrows pointing these areas. Each of these areas has a thickness of approximately 3 cm.

5.2.4 Atmospheric conditions

The atmosphere parameters for this simulation will be taken from the MODTRAN model, with the built-in parameters for a tropical environment, a visibility of 23 km, and the maritime aerosol profile. The ambient temperature for this environment is 300 K at sea level.

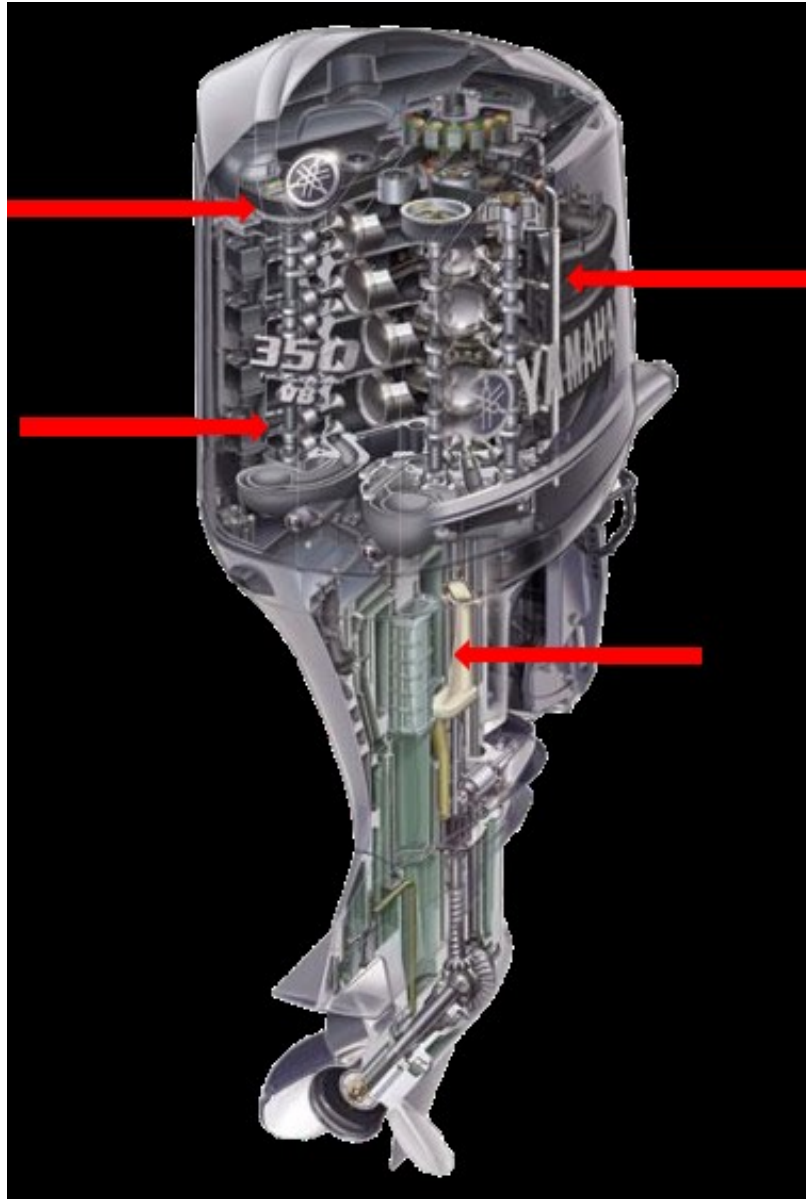


FIGURE 5.4 YAMAHA® V8 Offshore model F350. Adapted from [14]. The red arrows indicate the sensible areas to target the HEL weapon.

TABLE 5.2 Target material parameters. Adapted from [15, 7, 16, 17, 18].

Parameter	Material			
	Aluminum	Stainless Steel	Fiberglass composite	Rubber
Density (ρ) [kg/m ³]	2700	7900	900	1100
Melt Temperature (T_m)[K]	933	1700	600	405
Latent Heat of fusion (L) [J/kg]	3.97×10^5	3×10^5	1000	71400
Thermal conductivity in solid state (k_s) [W/m·K]	226	17	0.3	0.045
Thermal conductivity in liquid state (k_l) [W/m·K]	92	30.4	0.3	0.045
Thermal diffusivity in solid state (D_s) [m ² /s]	96.8×10^{-6}	4×10^{-6}	1.33×10^{-7}	0.89×10^{-7}
Thermal diffusivity in liquid state (D_l) [m ² /s]	38×10^{-6}	4.9×10^{-6}	1.33×10^{-7}	0.89×10^{-7}
Operation Temperature (T_0) [K]	360	360	300	300
Absorptivity (A)	0.202	0.442	0.5	0.9
Thickness [cm]	3	3	0.2	0.5

THIS PAGE INTENTIONALLY LEFT BLANK

Simulations Results

By running the ANCHOR code with the parameters mentioned in the last chapter, we obtained plots describing the interactions between the laser and the target materials for each situation. The results presented in this chapter assume the engagement of just one target (e.g. a single outboard motor). The watercraft used for these illegal activities typically have more than one motor; the time needed to fully disable the watercraft can be easily extrapolated by multiplying these dwell time results by the number of motors.

6.1 Surface Platform

The surface platform has the advantage of a larger capacity for energy storage and output power. Hence, we consider up to a 100 kW laser for this case. However, it operates at sea level, which makes it more exposed to extinction and turbulence effects than an aerial platform. Also, the surface platform is slower compared to the target, which will limit its potential engagement time and cross range.

6.1.1 Irradiance

As seen in Figure 6.1, the irradiance delivered drops off rapidly with distance due to atmospheric attenuation, diffraction and other effects. However, even the smallest simulated output power (10 kW) delivers irradiance on the order of megawatts per square meter at a distance of 3 km. The irradiance on target scales approximately linearly with laser output power. Since thermal blooming effects are not significant for output powers below 100 kW, they do not affect these simulations.

6.1.2 Power in the bucket

For an assumed bucket radius of 5 cm, the power deposited in this area scales as expected, as shown in Figure 6.2. At close distances, the power-in-the-bucket is approximately equal

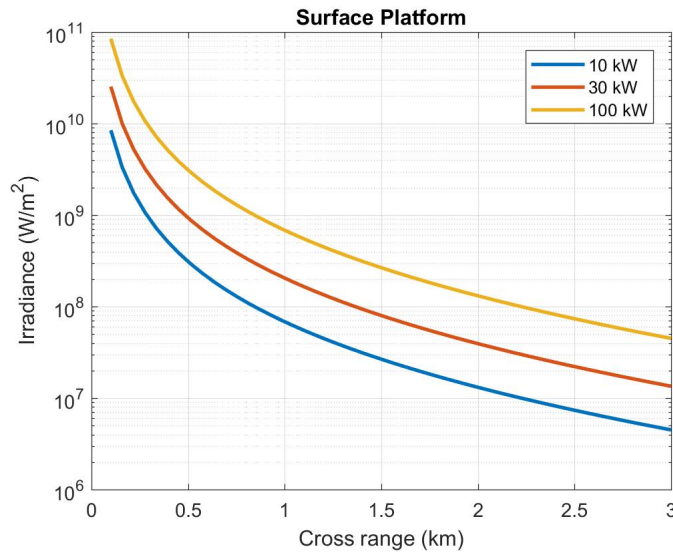


FIGURE 6.1 ANCHOR results for irradiance versus cross range to the target, for various laser output powers fired from a surface platform.

to the output power, since the laser spot remains completely inside the bucket and there is little atmospheric attenuation for cross ranges of less than a few hundred meters. At further distances, the power in the bucket drops approximately linearly for all the output powers as atmospheric effects become more significant. Also, as in the case of irradiance, the power in the bucket scales approximately linearly with output power.

6.1.3 Melt depth

In section 3.2 we discussed the interactions between the laser and the material during the melting process. The results shown in Figure 6.3 show the melt depth reached after a 1 second dwell time at different cross ranges for each laser output power.

In the case of the metals (aluminum and stainless steel) we see that, due to the short dwell time simulated, they do not even reach the melting point at longer cross ranges. The insulator materials (fiberglass and rubber) reach smaller melt depths than the metals at closer ranges because of their higher heat capacities; however, since they have smaller thermal conductivities and lower melting points than the metals, the melting thresholds are still crossed at longer ranges.

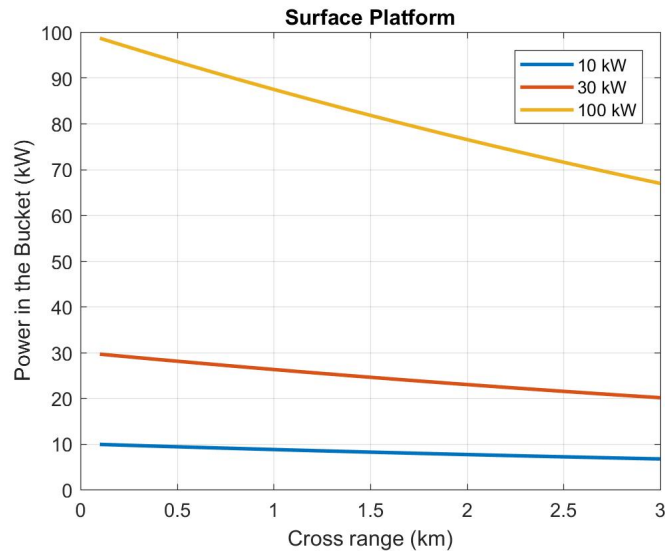


FIGURE 6.2 ANCHOR results for power in the bucket versus cross range to the target, for various laser output powers fired from a surface platform.

6.1.4 Dwell time

In Figures 6.4, 6.5, and 6.6, we plotted the required dwell time to melt through a given material thickness versus cross range, up to 3 km, for each one of the output powers considered for the surface platform. The dwell times include the time it takes the material to reach the melting point and the additional time required to melt through the materials. The thicknesses and physical properties for each material are given in table 5.2. Using these plots, we can estimate how long it would take to disable each target at a given cross range.

The surface platform simulated in this study is slower compared to the target. Thus, we are interested in engagements at the longest ranges possible since close approach is physically difficult due to the target being faster than the platform.

If the target's fuel lines are accessible, it would take less than 5 seconds for each of the output powers simulated to cut through one fuel line at the largest cross range (3 km), as shown in Figure 6.4. Therefore, all the considered output powers would be viable in this case.

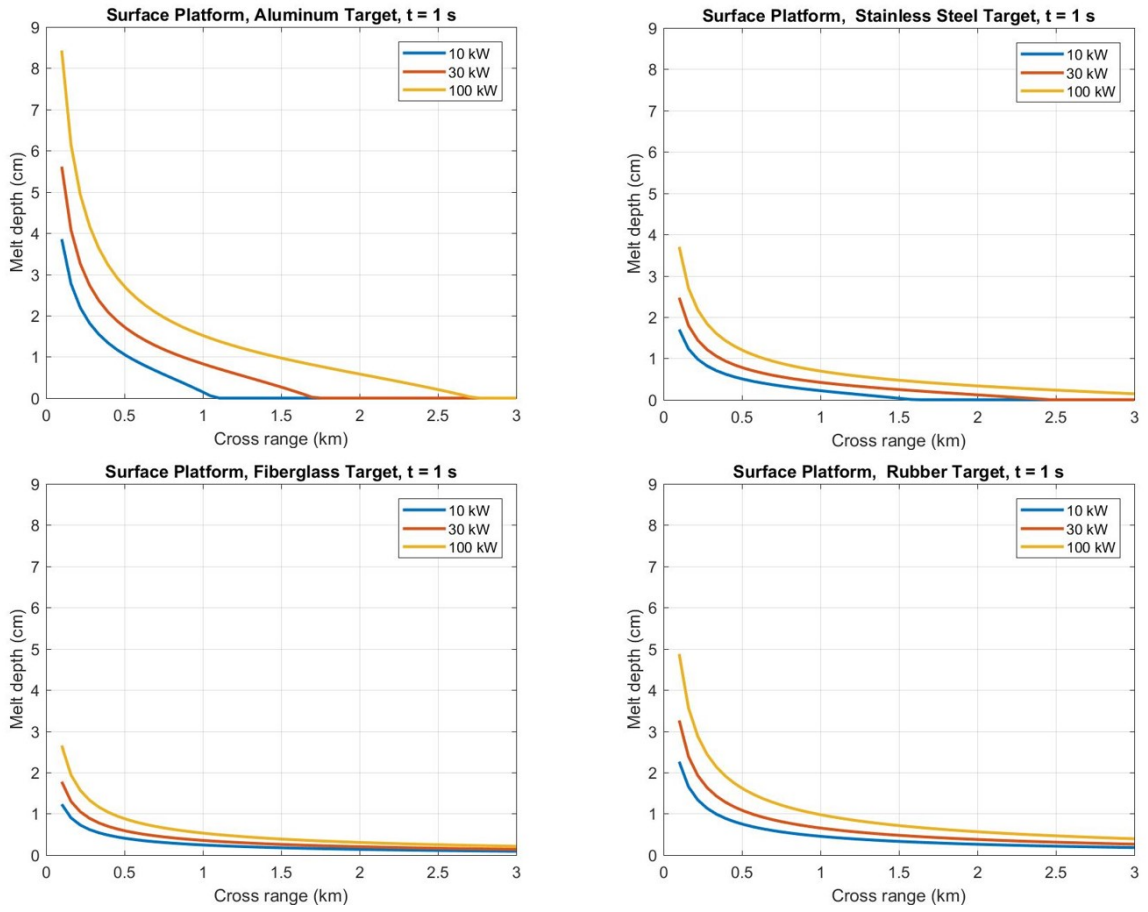


FIGURE 6.3 ANCHOR results for melt depth versus cross range at a dwell time of 1 second from a surface platform.

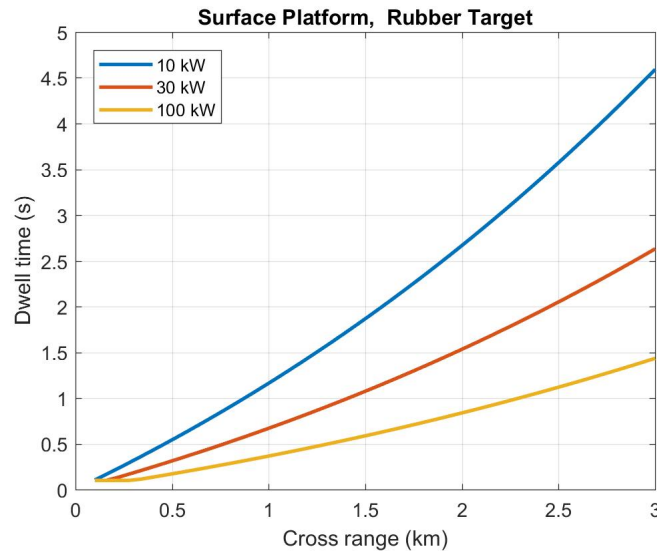


FIGURE 6.4 ANCHOR results for required dwell time to melt through a 5 mm thick rubber target versus cross range from a surface platform.

If the fuel lines are not accessible and we have to aim the weapon at the motor dome, the laser weapon would have to first melt through the fiberglass casing of the motor. In Figure 6.5 we see how, in this first part of the target, it takes less than 3.5 seconds for each of the output powers to melt through the casing at the largest cross range (3 km).

After the fiberglass casing, the laser needs to melt through the metallic motor parts. The plots for these two metallic target materials are shown in Figure 6.6. For an aluminum target, we see that the lowest simulated output power (10 kW) would need more than 100 seconds to melt through the thickness needed to disable the target at the longest cross range; it can be effective at closer ranges but, as said before, these ranges are unlikely due the platform speed limitations. However, the 100 kW device can disable one target in less than 20 seconds for a 3 km cross-range. For a multi-motor watercraft, the limited engagement window means that only the 100 kW device would likely be viable at the longest ranges.

The stainless steel target requires even more time to melt through at 3 km ranges. This further emphasizes the need for a 100 kW-class device.

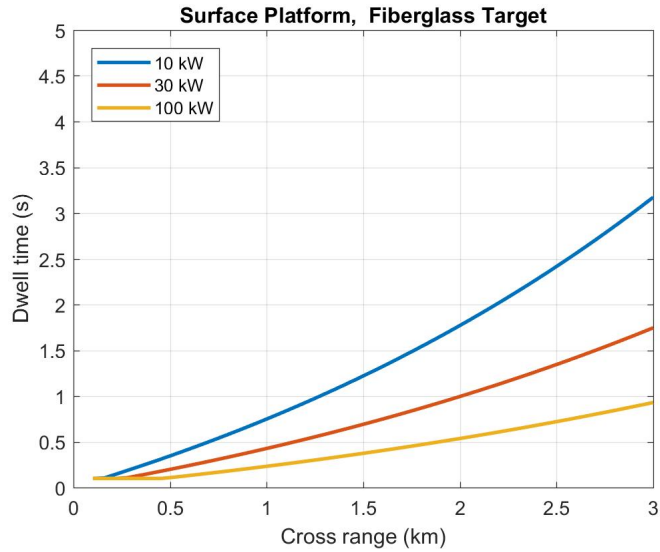


FIGURE 6.5 ANCHOR results for required dwell time to melt through a 2 mm thick fiberglass target versus cross range from a surface platform.

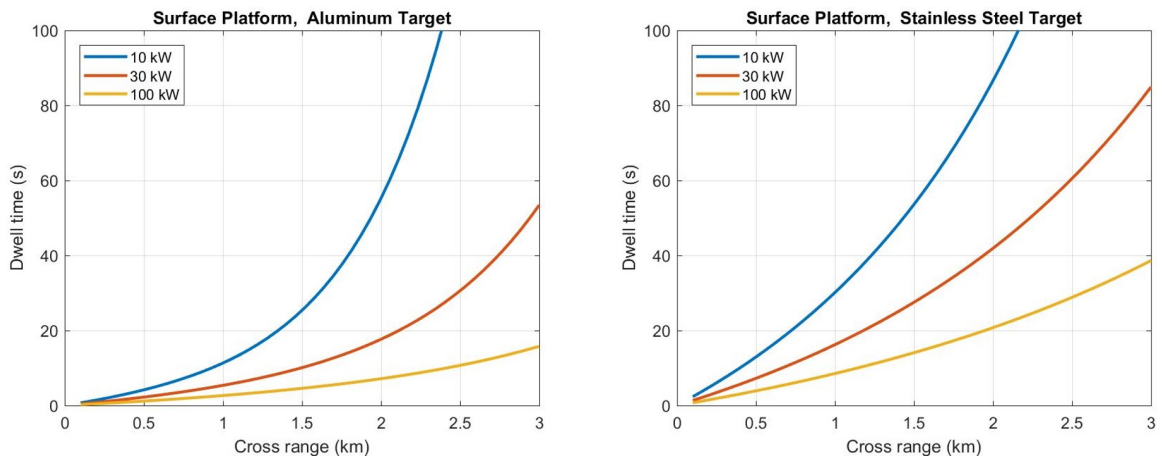


FIGURE 6.6 ANCHOR results for required dwell time to melt through a 3 cm thick metallic target versus cross range from a surface platform.

6.2 Unmanned Aerial Vehicle (UAV) Platform

The UAV platform has the advantage of higher altitude, which makes it less exposed to turbulence effects. Nevertheless, it presents limitations in the size, weight, and power of the weapon it may carry due to take-off weight and endurance considerations [19], thus we only consider output powers up to 50 kW. Also, the UAV platform is faster compared to the target, which lets it get closer to the target and fly circular patterns around it. This diminishes the atmospheric losses of the laser beam by engaging at closer ranges and/or allows the laser to engage for longer dwell times .

6.2.1 Irradiance

As in the case of the surface engagement, the irradiance delivered drops off rapidly with distance due to diffraction and other effects, as shown in Figure 6.7. Even the smallest simulated output power (10 kW) delivers irradiance on the order of megawatts per square meter at a distance of 3 km. However, as stated before, this platform can engage the target at closer ranges. The smallest output power considered (10 kW) results in an irradiance on the order of tens of megawatts per square meter at a distance of 1 km. As seen in Figure 6.7, the irradiance on target scales approximately linearly with output power. Like before, thermal blooming effects are expected to be negligible.

6.2.2 Power in the Bucket

For an assumed bucket radius of 5 cm, the results plotted in Figure 6.8 follow the same trends as seen for the surface platform. However, unlike the results obtained with the surface platform, the results at closer ranges have a flatter slope because the actual distance covered by the laser beam is not the cross range, but the hypotenuse of the triangle formed by the cross range and the altitude of the platform. That hypotenuse does not change rapidly at cross ranges close to the target.

6.2.3 Melt depth

Like in the surface engagement section, the results shown in Figure 6.9 give us an idea of how the interactions between the laser beam and the materials affect the simulations performed in this study. These plots show the melt depth reached after a 1 second dwell time at different cross ranges for each laser output power. The observed trends here are the same as what was seen for the surface platform for all the materials.

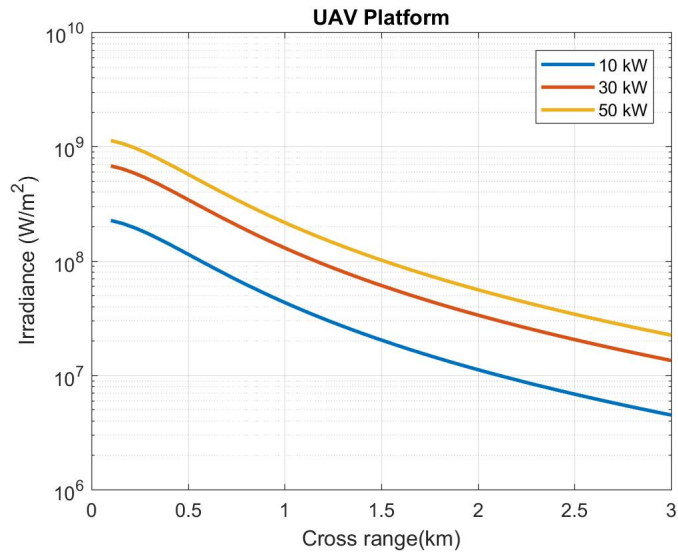


FIGURE 6.7 ANCHOR results for irradiance versus cross range to the target, for various laser output powers fired from a UAV platform.

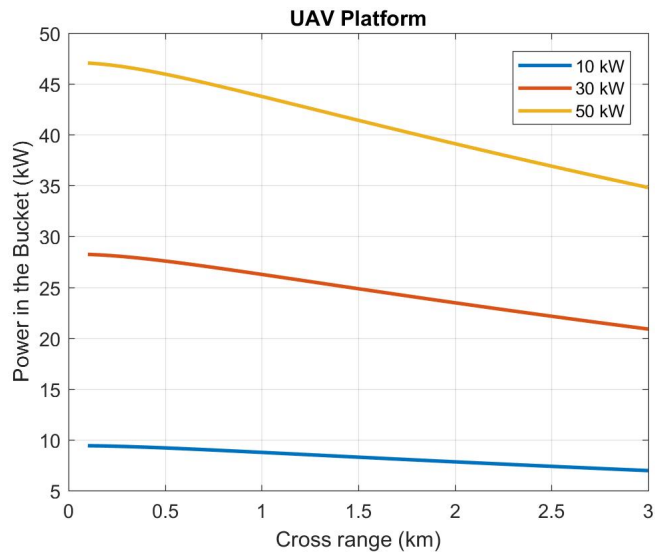


FIGURE 6.8 ANCHOR results for power in the bucket versus cross range to the target, for various laser output powers fired from a UAV platform.

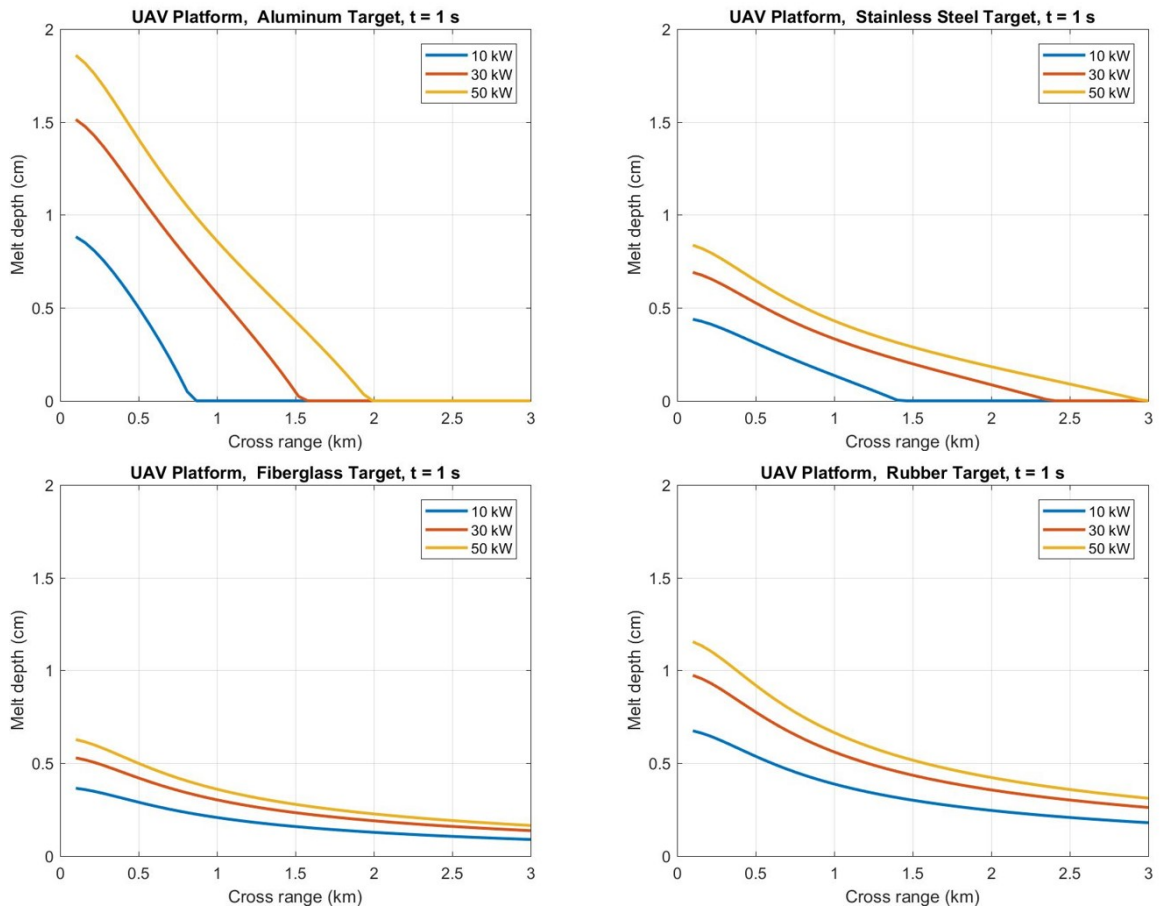


FIGURE 6.9 ANCHOR results for melt depth versus cross range at a dwell time of 1 second from a UAV platform

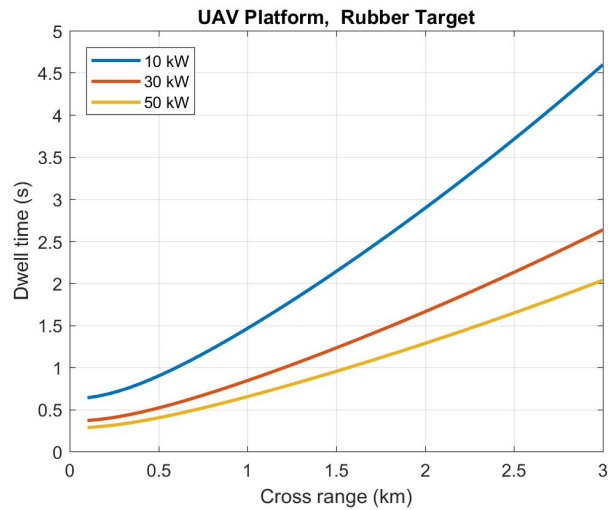


FIGURE 6.10 ANCHOR results for required dwell time to melt through a 5 mm thick rubber target versus cross range from a UAV platform.

6.2.4 Dwell time

In Figures 6.10, 6.11, and 6.12, we plotted the required dwell time to melt through a given material thickness versus cross range, up to 3 km, for each one of the output powers considered for the UAV platform. The dwell times include the time it takes the material to reach the melting point and the additional time required to melt through the materials. The thicknesses and physical properties for each material are given in table 5.2. Using these plots, we can estimate how long it would take to disable each target at a given cross range.

The UAV platform simulated in this study is faster compared to the target. Thus, we can look at engagements at closer ranges and tolerate longer dwell times.

If the target's fuel lines are accessible, it would take less than 5 seconds for each of the output powers simulated to cut through one fuel line at the largest cross range (3 km) as shown in Figure 6.10; even better, at 1 km cross range, it would take less than 2 seconds. Therefore, all the considered output powers would be viable in this case.

If, instead, we have to aim the weapon at the motor dome, we can see from Figures 6.11 and 6.12 that it takes a total of 20 seconds to melt through the fiberglass casing and aluminum

engine block at 1 km for the 10 kW device. For the stainless steel engine block it would take approximately 40 seconds to obtain the same effect. Thus, taking advantage of the platform speed to reduce the cross range and increase the engagement window makes any of the considered output powers viable. However, as for the surface platform, the relatively longer dwell times may offer a design challenge for the power and heat management of the weapon.

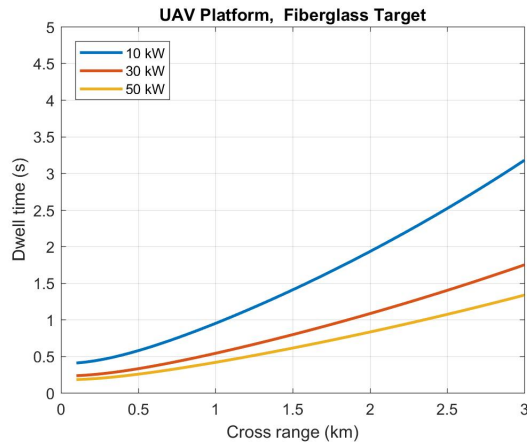


FIGURE 6.11 ANCHOR results for required dwell time to melt through a 2 mm thick fiberglass target versus cross range from a UAV platform.

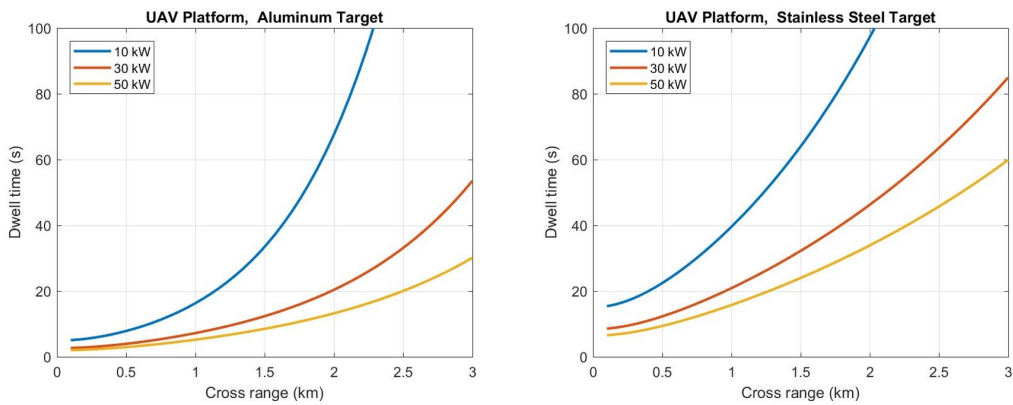


FIGURE 6.12 ANCHOR results for required dwell time to melt through a 3 cm thick metallic target versus cross range from a UAV platform.

THIS PAGE INTENTIONALLY LEFT BLANK

CHAPTER SEVEN

Conclusions

In the relevant interdiction scenarios for the Peruvian Navy, we found that it is feasible to use lasers with the output powers simulated in this study; however, the required power would depend on the platform where the weapon is installed. If installed on a surface platform, the output power of the weapon should be at least 100 kW because of the speed limitations of this platform. This ensures an effective interdiction at the longer cross ranges and shorter engagement windows this platform would likely encounter.

On the other hand, in a UAV platform, we can install weapons with an output power as low as 10 kW because it can achieve closer cross ranges due to its speed and has longer engagement windows. Also, weapons with these smaller output powers might be more feasible to install in this kind of platform because the inherit size and weight limitations of the platform.

For both platforms (and especially for the UAV), power and heat management issues may present further limitations on the dwell times. These power and size considerations have not been pursued in any great detail for this study, so research into this area represents a natural extension to this project.

THIS PAGE INTENTIONALLY LEFT BLANK

List of References

- [1] "Mision de la Marina de Guerra del Peru." Marina de Guerra del Peru. Accessed September 15, 2017. [Online]. Available: <https://marina.mil.pe/en/nosotros/acerca-de/>
- [2] United Nations Office on Drugs and Crime. "World drug report 2016". Vienna, Austria, 2016. [Online]. Available: http://www.unodc.org/doc/wdr2016/WORLD_DRUG_REPORT_2016_web.pdf
- [3] "Directed energy overview," class notes for Electric Ship Weapons System, Dept. of Physics, Naval Postgraduate School, Monterey, CA, fall 2016.
- [4] G. P. Perram, S. J. Cusumano, R. L. Hengehold, and S. T. Fiorino, *An Introduction to Laser Weapon Systems*. Albuquerque, NM, USA: Directed Energy Professional Society, 2010.
- [5] J. H. Valiani. "Power and energy storage requirements for ship integration of solid-state lasers on naval platforms". M.S. thesis, Dept. of Physics., NPS, Monterey, CA, USA, 2016. [Online]. Available: <https://calhoun.nps.edu/handle/10945/49406>
- [6] D. Sands, *Pulsed Laser Heating and Melting, Heat Transfer, Engineering Applications*, V. Vikhrenko, Ed. Rijeka, Croatia: InTeck, 2011.
- [7] J. Xie and A. Kar, "Mathematical modeling of melting during laser materials processing," *Journal of Applied Physics*, vol. 81, no. 7, pp. 3015–3022, 1997. Available: <https://doi.org/10.1063/1.364336>
- [8] Z. Shen, S. Zhang, J. Lu, and X. Ni, "Mathematical modeling of laser induced heating and melting in solids," *Optics & Laser Technology*, vol. 33, no. 8, pp. 533 – 537, 2001. Available: <http://www.sciencedirect.com/science/article/pii/S0030399201000056>
- [9] J. D. Exline, A. S. Levine, and S. S. Levine. (2008, Aug.). "Meteorology: An educator's resource for inquiry-based learning for grades 5-9". NASA. [Online]. Available: https://www.nasa.gov/centers/langley/pdf/220485main_MeteorologyTeacherResource508.r5.pdf
- [10] K. Cohn, "Linear atmospheric propagation effects," unpublished.

- [11] P. Sprangle, J. R. Peñano, and A. Ting. "Propagation of high-energy lasers in a maritime environment". NRL Review, pp. 59-65, May 2004. [Online]. Available: https://www.nrl.navy.mil/content_images/2004Review.pdf
- [12] "Talarion MALE unmanned air vehicle (UAV)". Air Force Technology. Accessed November 2, 2017. [Online]. Available: <http://www.airforce-technology.com/projects/talarionuav/>
- [13] D. Figueira. "The military assets necessary to disrupt the illicit trades,". Drugtrade blog, September 12, 2015. [Online]. Available: <https://drugtrade.wordpress.com/2015/09/12/the-military-assets-necessary-to-disrupt-the-illicit-trades/>
- [14] "Yamaha Outboard Engines". Yamaha Motors. Accessed September 12, 2017. [Online]. Available: <http://www.yamaha-motor.com/>
- [15] M. S. Tsoi. "Modeling of thermal properties of fiber glass polyester resin composite under thermal degradation condition". M.S. thesis, Dept. of Mechanical and Aerospace Science., University of Central Florida, Orlando, FL, USA, 2011. [Online]. Available: <http://stars.library.ucf.edu/etd/1718/>
- [16] J. Unsworth and F. J. Duarte, "Heat diffusion in a solid sphere and fourier theory: An elementary practical example," *American Journal of Physics*, vol. 47, no. 11, pp. 981–983, 1979. Available: <https://doi.org/10.1119/1.11601>
- [17] Engineering ToolBox Database. [Online]. Available: www.engineeringtoolbox.com
- [18] S. Thomas, C. H. Chan, L. A. Pothen, K. Rajisha, and H. J. Maria, Eds., *Natural Rubber Materials* (Polymer Chemistry 1). London, UK: Royal Society of Chemistry, 2013, pp. 261.
- [19] A. Lionis. "Experimental design of a UCAV-based high-energy laser weapon". M.S. thesis, Dept. of Physics., NPS, Monterey, CA, USA, 2016. [Online]. Available: <https://calhoun.nps.edu/handle/10945/51574>

Initial Distribution List

1. Defense Technical Information Center
Ft. Belvoir, Virginia
2. Dudley Knox Library
Naval Postgraduate School
Monterey, California